Self-consistent solutions of electronic wave functions at GaAs–$Al_xGa_{1-x}As$ interfaces

Y. Rajakarunanayake and T. C. McGill
California Institute of Technology, Pasadena, California 91125

(Received 23 March 1987; accepted 23 April 1987)

We report the first study of the self-consistent electronic wave functions at a heavily doped GaAs–$Al_xGa_{1-x}As$ interface. The doping densities in the GaAs are between 10^{17} and 10^{19} cm^{-3}. These doping densities are characteristic of tunnel structure devices. The Schrödinger equation is solved self-consistently in the Hartree approximation. Some of the more important results of our calculations include the fact that there is only a single subband level in the well for a wide range of biases. This level is also fairly loosely bound (bound by a few meV) in spite of the fact that the notch at the interface is on the order of a 100 meV. In accumulation layers, the potential at the interface is somewhat similar to the non-self-consistent one. However, in depletion layers the self-consistent potential can be substantially different from the one obtained in the Thomas–Fermi approximation.

I. INTRODUCTION

In this paper we have studied the self-consistent potential, and the associated electronic wave functions that exist at heavily doped GaAs–$Al_xGa_{1-x}As$ interfaces. These interfaces occur very commonly in single-barrier, and double-barrier heterostructures made of GaAs and $Al_xGa_{1-x}As$.[1–3] For example, let us consider a single barrier structure which consists of GaAs electrodes and a $Al_xGa_{1-x}As$ barrier. To describe the tunneling of electrons through this barrier, we have to study the response of GaAs electrons to an applied voltage bias. When the applied-electric field is perpendicular to the interface, accumulation and depletion layers are formed at the interfaces of the barrier on either side. With the self-consistent theory developed here, we are able to account for band bending and the details of the screening charge near the interfaces. These self-consistent solutions given here are of major interest because band bending plays a major role in determining the tunneling current and other device properties.[3–6,13]

The first part of this paper discusses the details of the Hartree model, and the important elements of self-consistent calculations. In the next part we discuss the results obtained for accumulation layers, and depletion layers separately. Two representative accumulation layers, and two depletion layers are studied in detail to explain the general features of the solutions. For each of these cases, the corresponding wave functions, carrier densities, and the potentials are included in the figures. One of the aims of this paper is to compare the merits of the Thomas–Fermi theory versus the self-consistent theory. Thus the corresponding Thomas–Fermi results are also discussed along with those of the self-consistent theory. The last section of this paper constitutes a brief summary of the major results.

II. DESCRIPTION OF THE MODEL

In our investigations, we have used the self-consistent Hartree model[7–9] to treat the accumulation and depletion layers that are formed in GaAs–$Al_xGa_{1-x}As$ heterostructures when a potential bias is applied. Right from the beginning, we can isolate the two interfaces of the barrier and study each side separately, since the coupling between the two sides is exponentially small as far as the electrostatics of the problem is concerned. Here the conduction band electrons of the heavily doped GaAs at the Γ point are allowed to rearrange themselves to provide the screening of the external electric field. The motion of these electrons are assumed to be described by a simple effective mass Schrödinger Hamiltonian. Since the Γ point of GaAs is isotropic, we can characterize the effective mass m^* by a simple scalar quantity.

In the Hartree approximation, each electron moves in the average electrostatic potential produced by all the other conduction electrons, and the uniform positive background due to the ionized donors. However, the forces acting on the electrons can be separated into two categories. The first category is the coulombic electrostatic forces that are accounted correctly by the Hartree term. The other category is the exchange and correlation forces that arise due to the statistics of spin $\frac{1}{2}$ Fermions. In principle these exchange terms have to be included in the Hamiltonian to correctly describe the motion of the electrons. However inclusion of these terms usually constitutes a many-body problem, and cannot be adequately described by an independent electron picture. The strength of the exchange–correlation force compared to the electrostatic force depends on the parameter r_s of the medium. Here r_s is the interelectronic spacing expressed in the units of the effective Bohr radius. Thus for heavily doped materials with high dielectric constants and low effective masses, we can argue that the exchange terms are subdominant. Fortunately, heavily doped GaAs has a small effective mass and a large dielectric constant, and thus we can be contented with only including the Hartree term of the potential in the Hamiltonian. The various approximate methods available for estimating these exchange and correlation potentials as functionals of the local-electron density, that go under the name of "density functional methods" will not be discussed here.[12] We have also ignored the electrostatic image forces that arise near the interface due to the difference in

 0734-211X/87/041288-07$01.00

the dielectric constants of the two materials.

In our model the GaAs–$Al_xGa_{1-x}As$ interface is assumed to be sharp. This enables us to treat the potential seen by the conduction band electrons of GaAs near the interface as a simple potential step with the appropriate magnitude of the conduction-band offset. The band offsets that occur in our structures are usually about 200 meV. This corresponds to an $Al_xGa_{1-x}As$ layer with a value of $x \approx 0.3$. We have also limited our attention to degenerately doped n-type GaAs electrons, at zero temperature. However a similar analysis can be performed on p-type semiconductors, and other direct gap materials, with only minor modifications to account for the finite temperatures. The effective mass of GaAs used is $m^* \approx 0.065 m_e$, where m_e is the bare electronic mass. The effective mass of $Al_xGa_{1-x}As$ used is $m^* \approx 0.092 m_e$. The background material (filled-valence electrons and ion cores) is assumed to be passive except to provide the uniform dielectric constant of the medium. In GaAs $\epsilon \approx 13.1\epsilon_0$, where ϵ_0 is the permittivity of the vacuum. In $Al_xGa_{1-x}As$ $\epsilon \approx 12.2\epsilon_0$.

The potential V is chosen to be zero far away from the interface, on the GaAs side. When the GaAs is attached to the negative electrode, electrons see an attractive potential, near the barrier. Thus an accumulation layer forms, and the potential is lowered below zero at the interface. However, when the GaAs is attached to the positive electrode, then a repulsive potential is formed at the barrier. In this case a depletion layer is formed and the potential is raised above zero near the barrier. We have chosen the z axis to be perpendicular to the interface. Thus, taking into account that there is no variation of the potential in the x–y plane, one can readily reduce this problem into a one-dimensional one. However, in matching the boundary conditions at the interface, the parallel component of the wave vector of each electron $k_{\|}$ is assumed to be conserved across the interface. When solving the self-consistent problem in the accumulation region, one also has to consider the bound states that can occur in the potential well.

In a typical self-consistent iteration scheme, we start with a guess for the form of the potential, and solve the one-dimensional Schrödinger equation. From these solutions, we then compute the charge density due to all the other conduction electrons, and the positive background. Using the charge density computed in the last step, we next solve the Poisson equation to obtain a new potential. The details of the various schemes used to achieve the convergence will not be discussed here.[10] A simple-minded scheme that works with considerable success is to modify the input potential by feeding back a fraction of the difference between the output and the input potentials of the last iteration.[8] We have found that an exponentially decaying potential with the appropriate Thomas–Fermi decay length works as a very good initial guess for starting the self-consistent iteration scheme.

In this section, we illustrate the solution of the Schrödinger equation in the effective mass approximation, for a guess Hartree potential $V(z)$. With the above assumptions, we can write the wave functions for this problem as $\psi(z)e^{ik_x x}e^{ik_y y}$. The resulting solutions, $\psi(z)$ are the set of envelope wave functions, in the z direction. The actual wave functions are a product of these envelope functions, and the appropriate microscopic Bloch functions. We have measured the energy E_k of the electron also with respect to the zero of the potential. If we introduce $q = k_z$ to simplify the formulas, then we can write

$$E_k = \frac{\hbar^2}{2m^*}(k_x^2 + k_y^2) + \epsilon_q ,$$

where

$$\epsilon_q = \frac{\hbar^2 q^2}{2m^*} = \frac{\hbar^2 k_z^2}{2m^*} .$$

Substituting these relations into the three-dimensional Schrödinger equation gives us the familiar one-dimensional Schrödinger equation

$$-\frac{\hbar^2}{2m^*}\frac{d^2}{dz^2}\psi_q(z) + V(z)\psi_q(z) = \epsilon_q \psi_q(z) .$$

When we solve this equation for positive energy by the above-described method, we consider incident waves impinging on the barrier from infinity, that reflect back from the barrier with only a negligible transmitted component. The boundary conditions are such that the exponentially increasing solution in the barrier is discarded. At the interface, we have also matched the boundary conditions that the current and the amplitude of each wave function be the same on both sides of the interface. The incident and the reflected waves interact to give solutions of the form which have the asymptotic forms, $\psi_q \psi_q^* \sim \sin^2(qz - \eta)$, far from the barrier. The normalization of these continuum states have to be done with considerable care. Thus we introduce a macroscopic normalization length L, and a cross-sectional area A for the bulk of GaAs in the tunnel structure, and let $L \to \infty$ at a later point of the calculation. Then we choose

$$\psi_q(z) \sim \sqrt{2/L}\,\sin(qz - \eta)$$

as $z \to \infty$. Each state $\psi_q(z)$ we obtain is the only allowed linear combination of $+q$ and $-q$ states. So we have to sum only over one-half of the Fermi sphere with $q > 0$ to obtain the charge distribution. When there are bound states, we also normalize their wave functions $\psi_b(z)$ by the condition

$$\int_0^\infty \psi_b^*(z)\psi_b(z)dz = 1$$

for each bound state. Defining

$$\psi_q(z) = \sqrt{1/L}\,\varphi_q(z)$$

we can write the contribution to the charge density from the mobile states as

$$\rho_{\text{mob}}(z) = -\frac{2e}{(2\pi)^3}\int_0^{k_F} \pi(k_F^2 - q^2)\varphi_q^*(z)\varphi_q(z)dq$$

after dividing out by the factor A (cross-sectional area). Introducing $u = q/k_F$, we can write this expression as

$$\rho_{\text{mob}}(z) = -\frac{ek_F^3}{2\pi^2}\int_0^1 (1 - u^2)\varphi_u^*(z)\varphi_u(z)du .$$

Thus in the large z limit since the average value $\langle \varphi_u^*(z)\varphi_u(z) \rangle = 1$, we immediately recover the negative of the background doping density ρ_{bac}, giving a net charge density of zero at large distances away from the barrier. Here

$$\rho_{\text{bac}}(z) = \frac{ek_F^3}{3\pi^2}$$

for uniform doping. Similarly for bound states,

$$\rho_{\text{bou}}(z) = \frac{-ek_F^2}{2\pi} \sum_{i=1}^{n} \left(1 - \frac{E_i}{E_F}\right) \psi_b^*(z)\psi_b(z) ,$$

where n is the number of bound states in the well. Here E_i is the energy of the ith bound state, measured with respect to the zero of the potential. Thus the total charge on one side per unit area is

$$Q = \int_0^{L\to\infty} [\rho_{\text{bou}}(z) + \rho_{\text{mob}}(z) + \rho_{\text{bac}}(z)]dz$$

$$= \int_0^{\infty} \rho_{\text{tot}}(z)dz.$$

Notice that it is proper to let $L \to \infty$ here because at this point of the calculation all our formulas are expressed in terms of quantities independent of L. This excess charge Q per unit area is negative in accumulation layers, and positive in depletion regions, and is in fact a boundary condition of the problem. Now in order to find the potential, the total charge density $\rho_{\text{tot}}(z)$ is plugged into the Poisson equation and integrated,

$$\frac{d^2}{dz^2} v(z) = \frac{e}{\epsilon} \rho_{\text{tot}}(z).$$

Using $v(z)$ is different from $V(z)$ if a self-consistent solution is not found. Thus we iterate this scheme with different guesses $V(z)$, until the self-consistency condition $V(z) \equiv v(z)$ is satisfied to the desired numerical accuracy.

III. RESULTS

A. Accumulation regions

One important feature that we discovered in our calculations was that there is only a single-bound state in the GaAs–$Al_x Ga_{1-x}As$ accumulation well for a wide range of applied biases. This observation was confirmed for doping densities ranging from 10^{17} to 10^{19} cm^{-3}, when the applied potential drop in the layer was between 50–100 meV. We have also found that this bound state is very loosely bound. The typical binding energies that we observed usually amounted to <20 meV, and were about 5%–15% of the well depth. In retrospect, the evidence that there is only a single-bound state makes the application of the semiclassical theory to this problem invalid. The Thomas–Fermi semiclassical theory of screening is valid only in a regime where there are a large number of bound states in the well. This is the assumption that enables one to incorporate the extra bound electrons into the Fermi sea. The Wentzel–Kramers–Brillouin (WKB) approximation for eigenvalues predicts that the number of bound states n in a semiclassical well is given by

$$n \approx \int_0^{\infty} \sqrt{\frac{-2m^*V(z)}{\hbar^2}}\, dz .$$

Thus we see that the number of bound states $n \sim \sqrt{m^*}$. We could then argue that, in the GaAs system with a very small effective mass, one has to use a self-consistent model instead of the Thomas–Fermi model since the number of expected bound states in the well would be small. The discovery that $n = 1$ verifies this hypothesis and further indicates the importance of using a self-consistent model.

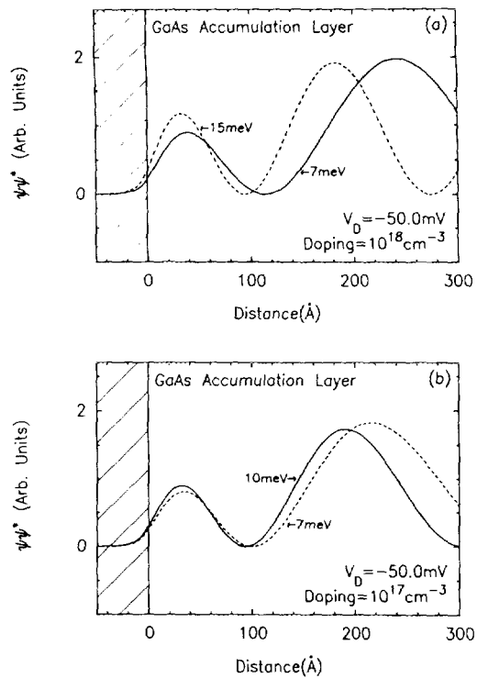

FIG. 1. Representative wave functions of accumulation layers. V_D is the potential drop in the GaAs layer. Note the decrease in the amplitude of $\psi\psi^*$ near the barrier. The respective energies of the electrons are indicated in meV. These curves are normalized to have an asymptotic form of $2\sin^2(qz - \eta)$ far away from the barrier. The energies are measured with respect to the conduction band edge at infinity.

In Figs. 1(a) and 1(b), we have shown the accumulation layer self-consistent wave functions of two typical unbound states. The doping density is 10^{18} cm^{-3} in Fig. 1(a) and 10^{17} cm^{-3} in Fig. 1(b). These are the wave functions of the mobile states when a potential difference of V_D is allowed to drop in the GaAs layer. In the graphs, the normalization of these states is done in such a way that far away from the barrier the value of $\psi_q\psi_q^*$ approaches $2\sin^2(qz - \eta)$. This normalization scheme allows us to compare the relative distortions that occur in each wave function as a function of energy and distance. In all these graphs, we definitely see a lack of negative charge near the barrier. The decaying exponential tail of these states gives rise to the tunneling current on the other side of the barrier. Thus it is very important to know the amplitude of these wave functions at the interface to accurately account for the tunneling current. We also see that, as the energy of the electrons is increased, their distortions from plane wave states is reduced. Thus the low lying conduction-band electronic states are the ones that are most distorted by the potential. Each solution here is constructed with an incoming wave and a reflected wave that is almost exactly in anti-phase with each other. (The phase difference would be exactly π if the barrier was infinite.) The definite phase difference between these two waves plays an important role in giving rise to a self-consistent charge density that

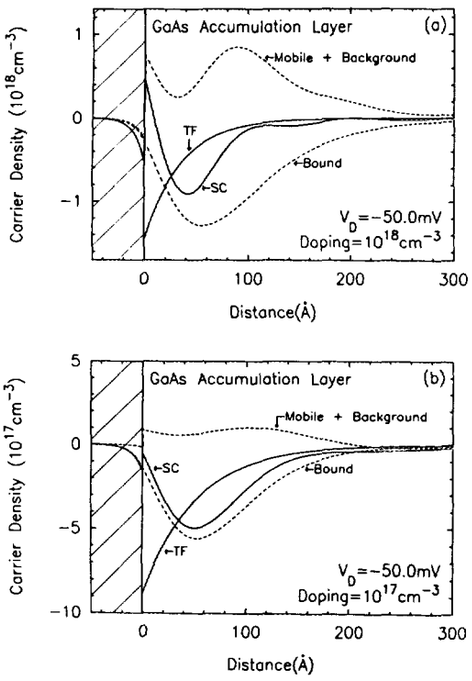

FIG. 2. Corresponding carrier densities obtained from the wave functions of Fig. 1. The self-consistent (SC) carrier density is the sum of the two curves mobile + background, and bound carrier densities. Notice that the self-consistent curve is very different from the Thomas–Fermi prediction. There is an excess of negative carriers, 5.7×10^{11} cm^{-2} in case (a) and 4.9×10^{11} cm^{-2} in case (b).

has Friedel type oscillations. However, when a scattering event occurs, the phase difference between these two waves would be randomized. Thus scattering would lead to an exponential decay in the Friedel oscillations of charge density. The length scale of this phenomenon can be estimated by assuming that scattering at low temperatures is predominantly charged impurity scattering. Realistically we can represent $\psi_q\psi_q^* \approx 1-\cos(2qz-2\eta)e^{-z/\lambda}$ in this case. Thus the definite phase relationship due to the reflection from the barrier would decay beyond a typical scattering length λ away from the barrier. A calculation we did with a crude model suggests that $\lambda \approx 1/k_F$. As these figures also illustrate, higher energy electrons penetrate more into the barrier, and thus would play a more important role in current conduction.

In Figs. 2(a) and 2(b) the dashed curves denoted by "bound" shows the bound state contribution to the charge density. All curves shown here correspond to the wave functions of Fig. 1. This bound charge arises from the two-dimensional subband of electrons that is bound in the GaAs accumulation well. This curve also resembles the shape of the wave function $\psi_b\psi_b^*$ of the bound state, since these two quantities are proportional to each other. The average spatial extent of these bound states is about 200–300 Å, and the peak of the bound state charge density occurs around 50–100 Å. These states show the expected trend that smaller binding energies results in states that have a larger spatial extent. The mobile state charge density plus the positive background charge density is shown as the dashed curve denoted "mobile + background." Thus when we are sufficiently far away from the barrier, the mobile state charge density and the positive background cancels each other out to give a neutral medium. One noticeable feature of the mobile state charge density is that it is depleted near the interface. Thus the dashed curve has a net positive charge density due to the dominant positive background near the interface. The reason for this lack of charge very near the barrier can be understood in terms of the boundary conditions that dictate exponential decay of the wave function inside the barrier. Thus, in accumulation layers as well as in depletion layers, the interference of the incoming and the reflected waves produced only a small amplitude of the wave function at the barrier. This is one of the major contrasts to the Thomas–Fermi theory of screening which predicts a charge density that also dips down to a maximum negative value at the interface. Figures 2(a) and 2(b) clearly show this difference between the charge densities of the Thomas–Fermi and self-consistent models. However, another reason for the lack of charge is that the mobile states have to be orthogonal to the bound state in this region. Thus, the presence of the bound state in the well expels the mobile state electrons further away from the well, causing a lack of charge (a hole-like state) in the vicinity of the bound state. This is purely an effect due to the orthonormalization of the mobile states with respect to the bound state. Both these effects gives rise to depletion of the mobile electrons away from the well region even in the accumulation layer. These curves also undergo abrupt jumps as they cross the barrier and enter the undoped AlAs side. This is merely an artifact of the disappearance of the background positive charge as we go from the doped-GaAs side to the undoped-$Al_xGa_{1-x}As$ side. We are also able to observe the fraction of the electron charge density that has penetrated inside the barrier in these curves.

The solid curve denoted SC (self-consistent) is the sum of the charge densities due to the positive background, bound electrons, and the mobile electrons, and is proportional to $\rho_{\rm tot}(z)$. This is the charge density that is used in the Poisson equation to determine the self-consistent potential. Another interesting feature of the self-consistent charge density curve in Fig. 2(a) is that there is a dipole layer at the interface that has an extent of about 20 Å on each side. However, in the low doping case of Fig. 2(b), we do not see the formation of such a dipole layer. The excess negative charge that produces the dip in the potential mainly comes from the bound state. The bound state charge density in this region is 2–5 times the magnitude of the background doping in Fig. 2(b). By comparing Figs. 2(a) and 2(b) we also see that the relative importance of the bound state in accounting for the charge density is greater in the low density 10^{17} cm^{-3} case than in the high density 10^{18} cm^{-3} case.

In Figs. 3(a) and 3(b) we see the potentials corresponding to the wave functions of Fig. 1, and charge densities of Fig. 2. The exceptional closeness of the self-consistent potential and the Thomas–Fermi potential is indeed surprising, considering that the resulting charge densities are quite different. One way of understanding this is to say that, the presence of the bound state in the well alters the unbound states

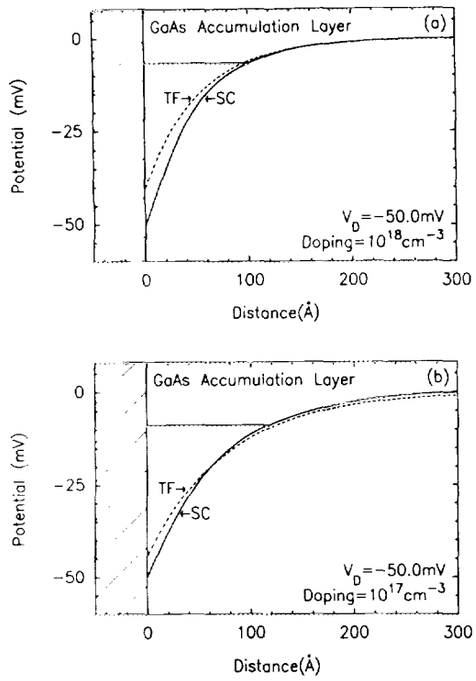

FIG. 3. Corresponding potential for Figs. 1 and 2 above. Notice the similarities between the Thomas–Fermi (TF) and self-consistent (SC) potentials in the accumulation layers. The bound states are very loosely bound, with binding energies of 5.8 meV in (a) and 11.6 meV in (b). The applied potential drop is 50 mV in (a) and (b).

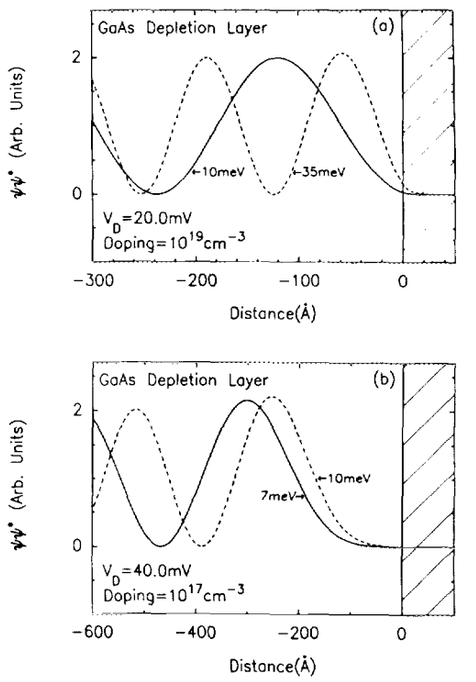

FIG. 4. Representative wave functions of depletion layers. V_D is the potential drop in the GaAs layer. Note that these states resemble plane waves in the depletion region, unlike in the accumulation region of Fig. 1. The respective energies of the electrons are indicated in meV. These curves are normalized to have an asymptotic form of $2\sin^2(qz-\eta)$, far away from the barrier. The energies are measured with respect to the conduction band edge at infinity.

wave functions so as to produce an orthonormalization hole in the conduction band.[7,11] This orthonormal hole-like state that exists in the conduction band moves in correlation with the bound state in response to external biases so as to make the total charge in the layer a continuous function of the applied bias. An analogous result has been proved by Kohn and Majumdar even in the event when the number of bound states in the well is variable. Thus, if a bound state vanishes at a certain strength of the applied bias, the significant fraction of charge that vanishes with it reappears in the conduction band as unbound charge. This corresponds to the rearrangement of charge that takes place due to the vanishing of the orthonormal hole. This enables one to lump the behavior of the bound state and the orthonormal holelike state from the continuum as a simple excess of charge that monotonically increases with the applied bias. This reduces to the same type of behavior that the Thomas–Fermi theory exhibits. This form of behavior, added to the constraint that the derivatives of the self-consistent and Thomas–Fermi potentials be equal at the interface (condition of same excess charge), would explain why the potentials look very similar. The position of the bound state that occurs in these wells is shown as the horizontal line segment in the figure.

B. Depletion regions

In Figs. 4(a) and 4(b) we see the wave functions of typical depletion layers. These are also normalized in the same way as in Figs. 1(a) and 1(b), to obtain their asymptotic forms of $2\sin^2(qz-\eta)$ to the far left-hand side of the barrier. Results are presented for a doping density of 10^{19} cm^{-3} in Fig. 4(a) and 10^{17} cm^{-3} in Fig. 4(b). These electrons are reflected before they hit the barrier due to the repulsive self-consistent potential, that bends upwards in these layers. Thus the component of their wave functions that penetrate into the barrier is vastly reduced from those in the accumulation layers. We also see that these solutions are much less distorted from plane waves than in the case of the accumulation layers. This lack of distortion can be attributed to the lack of the bound state on this side of the barrier. Thus there is no distortion due to the orthonormalization requirement. One other noticeable result is that these waves actually undergo a slight accumulation in the first half wavelength away from the barrier. Again this leads to Friedel oscillations in the charge density.

Figures 5(a) and 5(b) show the corresponding charge densities of the wave functions of Fig. 4. The solid line SC is the self-consistent charge density which is the sum of the mobile electron contribution and the background positive ion contribution. In Fig. 5(a) a very small potential drop (20 meV) is applied with a deficient charge density of 9.0×10^{11} cm^{-2}. On the other hand, in Fig. 5(b) a larger potential drop (40 meV) compared to the Fermi energy ($E_F = 12$ meV) is applied with a deficient charge density of 2.2×10^{11} cm^{-2}. Here we clearly see the long-range Friedel oscillations in the charge density that are characteristic of self-consistent calculations. They do not decay with an expo-

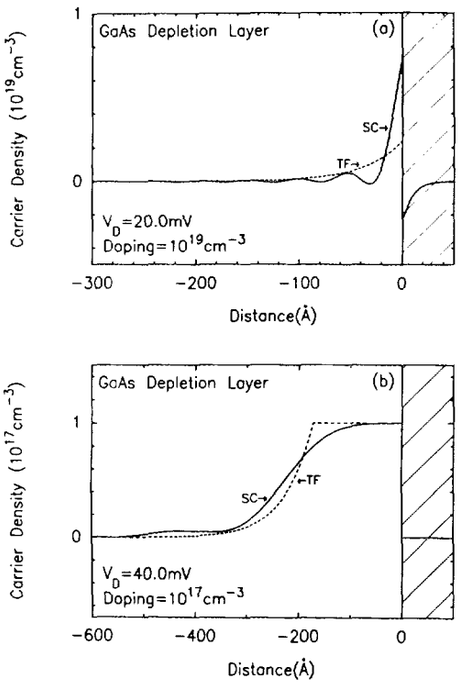

FIG. 5. Corresponding carrier densities obtained from the wave functions of Fig. 4. The self-consistent (SC) carrier density, and the Thomas–Fermi (TF) carrier density are quite different. Notice also the character of the long range oscillations of the self-consistent charge density. There is a deficiency of negative carriers, 9.0×10^{11} cm^{-2} in case (a) and 2.2×10^{12} cm^{-2} in case (b).

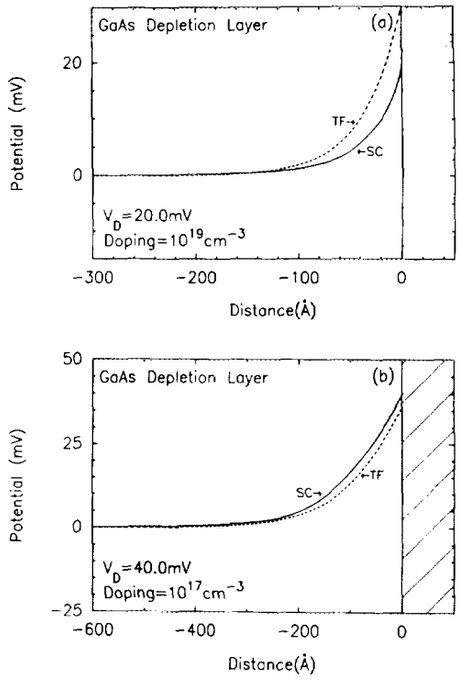

FIG. 6. Corresponding potential for Figs. 4 and 5 above. Note that in depletion layers, the self-consistent and Thomas–Fermi potentials can look very different from each other, as illustrated in case (a). The applied potential drop is 20 mV in (a) and 40 mV in (b).

nential decay envelope although their amplitudes are small. These oscillations are dominant at high-doping density, small applied positive bias, and low temperatures. From a physical point of view the long-range oscillations in the screening charge arises from a sharp Fermi surface. The reason is that it is not possible to construct a smooth function free of oscillations with the restricted set of waves $q < k_F$. Thus, the screening charge will always exhibit oscillations approximately at $2k_F$, twice the cutoff frequency. The self-consistent screening charge also has a decay envelope that dies as an inverse power law, in contrast to the Thomas–Fermi result that predicts an exponential decay rate. However, at finite temperatures, these Friedel oscillations die out with an exponential factor proportional to $k_B T$. Thus, in real systems at finite temperature, the significance of these oscillations is negligible. The figures compare the self-consistent charge density with the Thomas–Fermi charge density. In the fully depleted region which occurs in Fig. 5(b), these two charge densities resemble one another. However, in the region beyond this, the difference is significant. This is mainly due to the difference in the long-range screening properties predicted by the two theories. There is also no apparent dipole layer on this side of the barrier unlike in the accumulation layers.

In Figs. 6(a) and 6(b) the self-consistent potential corresponding to the wave functions of Fig. 4, and the charge density of Fig. 5 is shown. The self-consistent potential and the Thomas–Fermi potential for the depletion layers can be significantly different from each other. The agreement between these two curves is worse in depletion layers than in accumulation layers. The reason for this difference is the assumption that the charge gets depleted in an exponential manner with a Thomas–Fermi decay length is not a valid one. In fact, the screening charge decays in the Hartree case with an envelope function of an inverse power law as discussed above. We also discovered that the Thomas–Fermi solution lies above the self-consistent solution in highly doped cases, and below the self-consistent solution in lightly doped cases.

IV. CONCLUSION

In conclusion, we see that the Thomas–Fermi theory is quite good at describing the potential in accumulation layers although it does a poor job at describing the charge densities. Our results indicate that by assuming the actual potential to be given by the Thomas–Fermi form, and solving for its eigenstates and eigenvalues one can obtain answers that are very close to the self-consistent ones. Thus, calculating the charge density from the wave functions of the Thomas–Fermi potential is quite adequate for describing the current through the device, and calculating the positions of the bound levels. Hence, one does not have to go through a full-blown numerical self-consistent calculation to obtain reasonable results for the accumulation layers. On the other hand, the potential and charge density of the depletion layers can be quite different from the self-consistent one, and has to be treated more carefully. The results of this study also indicates that there are no other electron levels in the well of the accumulation region, except for a single loosely bound level.

This implies that we can theoretically expect the turning off of the negative resistance in double barrier structures to be quite sharp. The reason for this is that the only level in the accumulation layer below the band edge lies very close to the band edge. We expect the self-consistent solutions given here to play an important role in the understanding of tunneling of electrons in double and single barrier heterostructures.

ACKNOWLEDGMENTS

We would like to acknowledge G. Y. Wu, T. K. Woodward, and D. H. Chow for valuable discussions. Parts of this work was supported by ONR under Contract No. N00014-84-K-0501.

[1]R. Tsu and L. Esaki, Appl. Phys. Lett. **22**, 562 (1973).
[2]L. L. Chang, L. Esaki, and R. Tsu, Appl. Phys. Lett. **24**, 593 (1974).
[3]A. R. Bonnefoi, D. H. Chow, T. C. McGill, R. D. Burnham, and F. A. Ponce, J. Vac. Sci. Technol. B **4**, 988 (1986).
[4]A. R. Bonnefoi, D. H. Chow, and T. C. McGill, J. Appl. Phys. (to be published).
[5]H. Ohnishi, T. Inata, S. Muto, N. Yokoyama, and A. Sihbatomi, Appl. Phys. Lett. **49**, 1248 (1986).
[6]B. Ricco and M. Ya. Azbel, Phys. Rev. B **29**, 1970 (1984).
[7]G. A. Baraff and J. A. Appelbaum, Phys. Rev. B **5**, 475 (1972).
[8]T. Ando, A. B. Fowler, and F. Stern, Rev. Mod. Phys. **54**, 459 (1982).
[9]F. Stern and W. E. Howard, Phys. Rev. **163**, 816 (1967).
[10]F. Stern, J. Comput. Phys. **6**, 56 (1970).
[11]W. Kohn and C. Majumdar, Phys. Rev. A **138**, 1617 (1965).
[12]T. Ando, Phys. Rev. B **13**, 3468 (1976).
[13]T. Ando, J. Phys. Soc. Jpn. **51**, 3893 (1982).